

Performance improvement of magneto-acousto-electrical tomography for biological tissues with sinusoid-Barker coded excitation

Zheng-Feng Yu(余正风), Yan Zhou(周(龙天)), Yu-Zhi Li(李禹志), Qing-Yu Ma(马青玉), Ge-Pu Guo(郭各朴), Juan Tu(屠娟), Dong Zhang(章东)

Citation: Chin. Phys. B . 2018, 27(9): 094302. **doi:** 10.1088/1674-1056/27/9/094302

Journal homepage: http://cpb.iphy.ac.cn; http://iopscience.iop.org/cpb

What follows is a list of articles you may be interested in

Lorentz force electrical impedance tomography using pulse compression technique

Zhi-shen Sun(孙直申), Guo-qiang Liu(刘国强), Hui Xia(夏慧)

Chin. Phys. B . 2017, 26(12): 124302. **doi:** 10.1088/1674-1056/26/12/124302

Boundary normal pressure-based electrical conductivity reconstruction for magneto-acoustic tomography with magnetic induction

Ge-Pu Guo(郭各朴), He-Ping Ding(丁鹤平), Si-Jie Dai(戴思捷), Qing-Yu Ma(马青玉)

Chin. Phys. B . 2017, 26(8): 084301. **doi:** 10.1088/1674-1056/26/8/084301

Reception pattern influence on magnetoacoustic tomography with magnetic induction

Sun Xiao-Dong, Wang Xin, Zhou Yu-Qi, Ma Qing-Yu, Zhang Dong

Chin. Phys. B . 2015, 24(1): 014302. **doi:** 10.1088/1674-1056/24/1/014302

Conductivity reconstruction algorithms and numerical simulations for magneto-acousto-electrical tomography with piston transducer in scan mode

Guo Liang, Liu Guo-Qiang, Xia Hui, Liu Yu, Lu Min-Hua

Chin. Phys. B . 2014, 23(10): 104303. **doi:** 10.1088/1674-1056/23/10/104303

Performance improvement of magneto-acousto-electrical tomography for biological tissues with sinusoid-Barker coded excitation*

Zheng-Feng Yu(余正风)[1], Yan Zhou(周奘)[1], Yu-Zhi Li(李禹志)[1], Qing-Yu Ma(马青玉)[1,†], Ge-Pu Guo(郭各朴)[1], Juan Tu(屠娟)[2], and Dong Zhang(章东)[2]

[1] *Jiangsu Provincial Engineering Laboratory of Audio Technology, School of Physics and Technology, Nanjing Normal University, Nanjing* 210023, *China*
[2] *Institute of Acoustics, Nanjing University, Nanjing* 210093, *China*

(Received 28 May 2018; revised manuscript received 3 July 2018; published online 28 August 2018)

By combining magnetics, acoustics and electrics, the magneto-acoustic-electrical tomography (MAET) proves to possess the capability of differentiating electrical impedance variation and thus improving the spatial resolution. However, the signal-to-noise ratio (SNR) of the collected MAET signal is still unsatisfactory for biological tissues with low-level electrical conductivity. In this study, the formula of MAET measurement with sinusoid-Barker coded excitation is derived and simplified for a planar piston transducer. Numerical simulations are conducted for a four-layered gel phantom with the 13-bit sinusoid-Barker coded excitation, and the performances of wave packet recovery with side-lobe suppression are improved by using the mismatched compression filter, which is also demonstrated by experimentally measuring a three-layered gel phantom. It is demonstrated that comparing with the single-cycle sinusoidal excitation, the amplitude of the driving signal can be reduced greatly with an SNR enhancement of 10 dB using the 13-bit sinusoid-Barker coded excitation. The amplitude and polarity of the wave packet filtered from the collected MAET signal can be used to achieve the conductivity derivative at the tissue boundary. In this study, we apply the sinusoid-Barker coded modulation method and the mismatched suppression scheme to MAET measurement to ensure the safety for biological tissues with improved SNR and spatial resolution, and suggest the potential applications in biomedical imaging.

Keywords: magneto-acousto-electrical tomography, sinusoid-Barker coded excitation, mismatched compression filter, side lobe suppression

PACS: 43.80.Ev, 72.55.+s **DOI:** 10.1088/1674-1056/27/9/094302

1. Introduction

Significant differences in electrical impedance among different tissues or tissues in different pathological states were observed[1,2] in previous studies. It was reported that the conductivity of muscle was about ten times that of the fat tissue,[3] and the conductivity of breast cancer was much higher than that of the normal one.[4] Because of the wide variation range of electrical conductivity, images with improved contrast were achieved using electrical impedance tomography (EIT).[5,6] However, the spatial resolution and imaging depth of EIT are still limited by the shielding effect and the high-level current injection.[7] For the limited number of electrodes, the practical application of EIT is also hindered by the ill-posed inverse problem solution.[8] By combining the interaction among acoustic, magnetic and electrical fields, magneto-acousto-electric tomography (MAET),[9] also called Lorentz force impedance tomography[10,11] was proposed as an improved modality for mapping the distribution of electrical conductivity inside tissues. With the excitation of ultrasound and the detection of electrical signals in a static magnetic field, the merits of high spatial resolution and image contrast[12] of MAET have been demonstrated by theoretical and experimental studies in the past decades.

The origin of MAET is based on the principle of Hall effects imaging (HEI),[13,14] which was proposed by Han *et al.* With the excitation of a high-voltage pulse on an ultrasound transducer, images of the internal structure of plastic phantoms and tissue samples with apparent conductivity variations were restored. Then, the reciprocal method called magnetoacoustic tomography with magnetic induction (MAT-MI) was proposed by He *et al.*[15] and several algorithms were established for conductivity reconstruction both in the isotropic and anisotropic cases.[16–18] Based on the reciprocity theorem between electronics and acoustics, the MAET was also developed by Haider *et al.*[19] and the distributions of the induced current density inside the phantom were reconstructed. By applying the modified Wiener inverse filter and Hilbert transform to the collected MAET signal, the amplitude and polarity of conductivity variation were retrieved by Zhou *et al.*[20] and the one-dimensional distribution of conductivity along the acoustic transmission path was restored. In addition,

*Project supported by the National Natural Science Foundation of China (Grant Nos. 11474166 and 11604156), the Natural Science Foundation of Jiangsu Province, China (Grant No. BK20161013), the Postdoctoral Science Foundation of China (Grant No. 2016M591874), the Postgraduate Research & Practice Innovation Program of Jiangsu Province, China (Grant No. KYCX17_1083), and the Priority Academic Program Development of Jiangsu Provincial Higher Education Institutions, China.

†Corresponding author. E-mail: maqingyu@njnu.edu.cn

© 2018 Chinese Physical Society and IOP Publishing Ltd

some mathematical models and numerical frameworks were established for accurate conductivity reconstruction with the requirement for a higher signal-to-noise ratio (SNR) of collected signals.[21–23] The practical application of MAET was still hindered by the obvious drawbacks of low-level amplitude of the induced current and poor SNR of the collected MAET signal. In order to improve the performance of image reconstruction, a focused ultrasound beam was employed in practical measurements,[24] and the sectional impedance image for a beef sample was obtained with a high contrast. Although the difference frequency magneto-acousto-electrical tomography[25] was reconstructed by Renzhiglova *et al.* with a focused ultrasound excitation at the carrier frequency of 2.25 MHz and the modulated frequency of 2 kHz, the acoustic intensity in the focal zone was estimated at 37 W/cm^2, which is still far above the safety limit.

In the past decades, pulse compression technology originating from radar applications has been introduced into ultrasound imaging[26,27] to enhance the imaging depth and SNR with a longer time duration and a lower amplitude of acoustic excitation. The matched and mismatched filters were used to compress the bursts into a short interval pulse and suppress side lobes of received signals. Due to the improvement of SNR in ultrasound imaging, the linearly frequency modulated pulse[28,29] with an amplitude of 60 V was introduced into MAET by Sun *et al*. The spatial peak temporal average intensity of 17.4 mW/cm^2 was produced in the region of the sample and the discontinuous conductivity distribution with a spatial resolution of 1 mm was also obtained by the spectrum of the intermediate frequency signal. However, the polarity (direction) of conductivity variation was lost in Fourier transformation.[30] Except for the amplitude or frequency modulated technologies, several bi-phase coded excitation modalities[31] were also used to realize the effective pulse compression in ultrasonic imaging, such as the Barker code,[32] the Golay code,[33] etc. Compared with other schemes, the Barker code proved to have the lowest autocorrelation range of side-lobe level and the highest sensitivity for phase among the bi-phase codes with the same length.[34]

To enhance the energy of the incident acoustic signal in this study, the longest 13-bit sinusoid-Barker coded excitation is introduced into MAET and the mismatched compression filter is employed to suppress the noise-level of side lobes. The formula of the collected MAET signal with 13-bit sinusoid-Barker coded excitation is derived and simplified for the transducer with a strong directivity. Numerical simulations are conducted for a four-layered gel phantom with the 13-bit sinusoid-Barker coded excitation and the improved performance of wave packet recovery with the suppressed side-lobe level is obtained by using the mismatched compression filter, which is also demonstrated by the experimental measurements for a three-layered gel phantom. It is proved that with the 13-bit sinusoid-Barker coded excitation, the amplitude of the driving signal can be reduced to half that of the conventional single-cycle sinusoidal excitation with an SNR improvement of about 10 dB. The value and polarity of the conductivity derivative at the tissue boundary can be achieved by the amplitude and direction of the decompressed wave packet. In this study, we provide a comprehensive method of the 13-bit sinusoid-Barker coded modulation and the mismatched suppression scheme to MAET measurement for biological tissues with improved SNR and spatial resolution, and we also suggest the potential applications in biomedical imaging.

2. Principle and method

The schematic diagram of the MAET measurement system using sinusoid-Barker coded excitation is shown in Fig. 1. In a static magnetic field with a constant intensity B_0 along the y direction, a multi-layered phantom with the conductivity $\sigma(z)$ is immersed in distilled water with two plate electrodes placed on both sides to detect the time-varied electrical voltage generated inside the conductive medium. Driven by a Barker code modulated sinusoidal sequence, an ultrasound beam generated by the transducer transmits through the phantom, creating ion vibrations inside the object. Interacted with the static magnetic field, the positive and negative ions move toward the opposite sides of the phantom, producing the electrical potential between the plate electrodes.

In an in-viscous homogeneous medium, the particle velocity $\boldsymbol{v}$ satisfies the motion equation $\rho_0 \mathrm{d}\boldsymbol{v}/\mathrm{d}t = -\boldsymbol{\nabla} p$, where p is the acoustic pressure and ρ_0 is the density of the medium. For the planar piston transducer with the center frequency f and radius a located at $z = 0$, the velocity on transducer surface is $u = u_\mathrm{a}\exp(\mathrm{j}\omega t)$, where u_a and ω are the amplitude and the angular frequency of the acoustic wave. Thus, the acoustic pressure at (r, φ, z) in cylindrical coordinates can be described by

$$p(r,\varphi,z) = \frac{\mathrm{j}k\rho_0 c_0 u_\mathrm{a}}{2\pi}\int_0^{2\pi}\int_0^a \frac{\mathrm{e}^{\mathrm{j}(\omega t - kR)}}{R} r'\,\mathrm{d}r'\,\mathrm{d}\varphi', \qquad (1)$$

where $(r', \varphi', 0)$ represents an arbitrary point on the transducer surface, c_0 is the acoustic speed in the medium, $k = \omega/c_0$ is the wave number, and R is the distance from $(r', \varphi', 0)$ to (r, φ, z). The radiation pattern of the planar piston transducer is $D(\theta) = |2J_1(ka\sin\theta)/(ka\sin\theta)|$,[35] where $J_1(x)$ is the Bessel function of first order and θ is the radiation angle of the acoustic beam. For the experimental transducer with $f = 500$ kHz and $a = 20$ mm, $ka = 41.9$ is much larger than 1. The main lobe of the acoustic beam is in the narrow angle scope of $2\theta = \arcsin(0.61\lambda/a)$ of 5.2° and the influence of radiation side lobes can be ignored for much lower pressure. Hence, the acoustic propagation can be approximated as a straight line

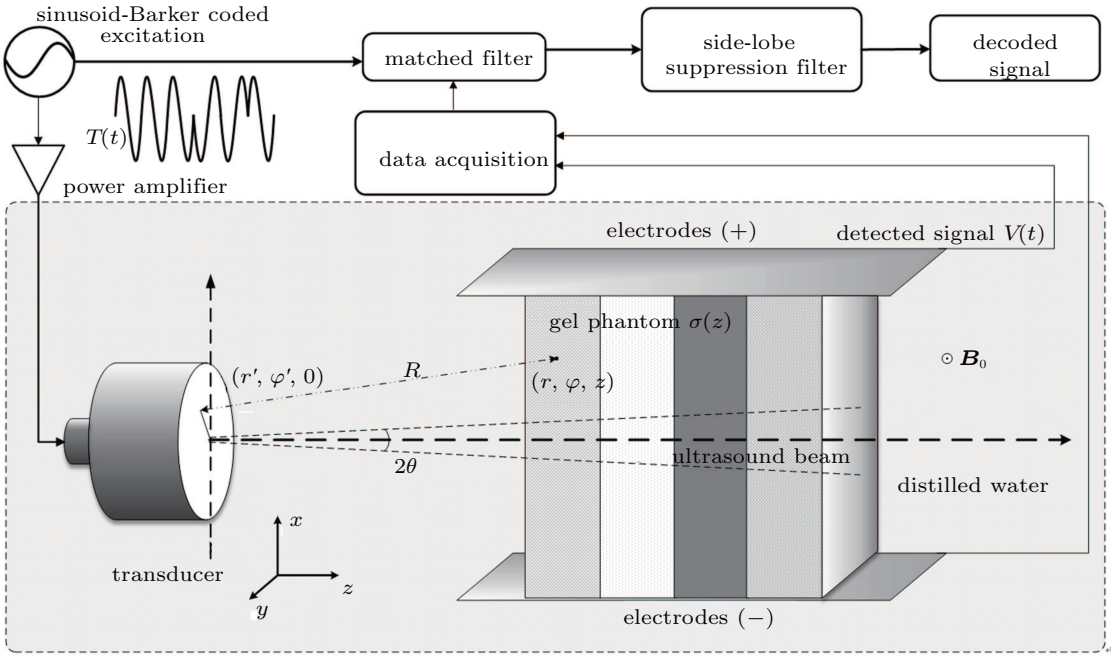


Fig. 1. Schematic diagram of MAET measurement system using sinusoid-Barker coded excitation.

along the z direction[20] and the acoustic pressure can be simplified into

$$p(r,\varphi,z)=\frac{\mathrm{j}\omega\rho_0 u_\mathrm{a}a^2}{2z}\mathrm{e}^{\mathrm{j}(\omega t-kz)}. \tag{2}$$

Then, the particle velocity of a charged particle can be calculated from $\boldsymbol{v}=-\int_0^t\nabla p\,\mathrm{d}t/\rho_0$. With the interaction between the static magnetic field and the ion vibration, the particle q is deflected by exerted Lorentz force $\boldsymbol{F}=q\boldsymbol{v}\times\boldsymbol{B}_0$, which is perpendicular to $\boldsymbol{v}$ and $\boldsymbol{B}_0$. During the acoustic propagation, a time-varying electrical field intensity $\boldsymbol{E}=\boldsymbol{v}\times\boldsymbol{B}_0$ is generated inside the tissue. Since the static magnetic field is in the y direction and the electrodes are in the x direction, only the z component of $\boldsymbol{v}$ contributes to the electrical field. Thus, the electrical field intensity can be approximated as

$$E_x=v_zB_0=-\frac{B_0}{\rho_0}\int_0^t\frac{\partial p}{\partial z}\mathrm{d}t$$

and the corresponding current density generated in the conductive medium can be calculated from

$$J_x=\sigma(z)\boldsymbol{v}\times\boldsymbol{B_0}=-\sigma(z)\frac{B_0}{\rho_0}\int_0^t\frac{\partial p}{\partial z}\mathrm{d}t. \tag{3}$$

By introducing the electrical collection factor β into the experimental system,[36] the collected MAET signal can be expressed as[20]

$$\begin{aligned}V(t)&=-\beta R_\mathrm{E}W\int_0^\infty J_x\mathrm{d}z\\&=-\frac{\beta B_0R_\mathrm{E}}{\rho_0}W\int_0^\infty\sigma(z)\mathrm{d}z\int_0^t\frac{\partial p}{\partial z}\mathrm{d}t,\end{aligned} \tag{4}$$

where W is the effective sectional area of the acoustic beam at the transmission distance z, and $R_\mathrm{E}=\int_{z_1}^{z_2}(1/\sigma(z))\mathrm{d}z$ is the equivalent electrical resistance of the entire model. By considering the absence of DC components of the practical ultrasound transducer,[9] the MAET signal can be simplified to[36]

$$\begin{aligned}V(t)&=\frac{\beta WB_0R_\mathrm{E}}{\rho_0}\int_0^\infty\int_0^t p\,\mathrm{d}t\frac{\partial\sigma(z)}{\partial z}\mathrm{d}z\\&=\frac{\beta WB_0R_\mathrm{E}a^2}{2}\int_0^\infty\frac{u(t-z/c)}{z}\frac{\partial\sigma(z)}{\partial z}\mathrm{d}z.\end{aligned} \tag{5}$$

The equation can also be rewritten as

$$V(t)=\frac{\beta WB_0R_\mathrm{E}a^2}{2}\frac{\partial\sigma(z)}{z\partial z}\otimes u(t),$$

meaning that the MAET signal is the convolution result between the conductivity derivative along the z direction and the surface velocity of the transducer. Considering the impulse response $R(t)$ of the transducer, the surface velocity $u(t)$ can be written as

$$u(t)=\xi R(t)\otimes T(t), \tag{6}$$

where ξ is the piezoelectric conversion efficiency of the transducer and $T(t)$ is the driving signal applied to the transducer. In this study, $T(t)=s(t)\otimes c(t)$ is the Barker coded sequence modulated with a single-cycle sinusoidal carrier, where $s(t)=\sin(2\pi ft)$ and $c(t)=\sum_{k=0}^{N-1}c_k\delta(t-kT_\mathrm{p})$ for $0\le t\le T_\mathrm{p}$, c_k denotes the amplitude of the Barker coded sequence, N is the length of the Barker code, and T_p is the time duration. The 13-bit Barker coded sequence and the corresponding sinusoid-Barker coded signal used in this study are plotted in Fig. 2(a).

Therefore, the formula of the MAET signal can be achieved as

$$V(t) = \xi' \frac{\partial \sigma(z)}{z \partial z} \otimes R(t) \otimes \left[\sin(2\pi f t) \otimes \sum_{k=0}^{N-1} c_k \delta(t - kT_\mathrm{p}) \right], \tag{7}$$

where $\xi' = \xi \beta W B_0 R_\mathrm{E} a^2/2$ is a constant coefficient determined by the experimental system.

A matched filter is employed to restore the output from the collected MAET signal, which is defined as the autocorrelation function of the sinusoid-Barker coded signal and expressed as $d(t) = T(t) \otimes T(-t)$. As shown in Fig. 2(b), the envelope of $d(t)$ is displayed as the same-shaped side lobes (-22.3 dB) spread around the main lobe symmetrically. However, in order to restore the wave packets at the conductivity boundaries, a filter with side-lobe level suppression over 40 dB is needed to satisfy the requirements for acceptable image contrast and spatial resolution. The mismatched compression filter is employed to suppress the side-lobe level of the sinusoid-Barker coded signal, whose transfer function in the frequency domain is presented as[37]

$$H(f) = \left(N - 1 + \frac{\sin 2\pi N f T_\mathrm{p}}{\sin 2\pi f T_\mathrm{p}} \right)^{-1}. \tag{8}$$

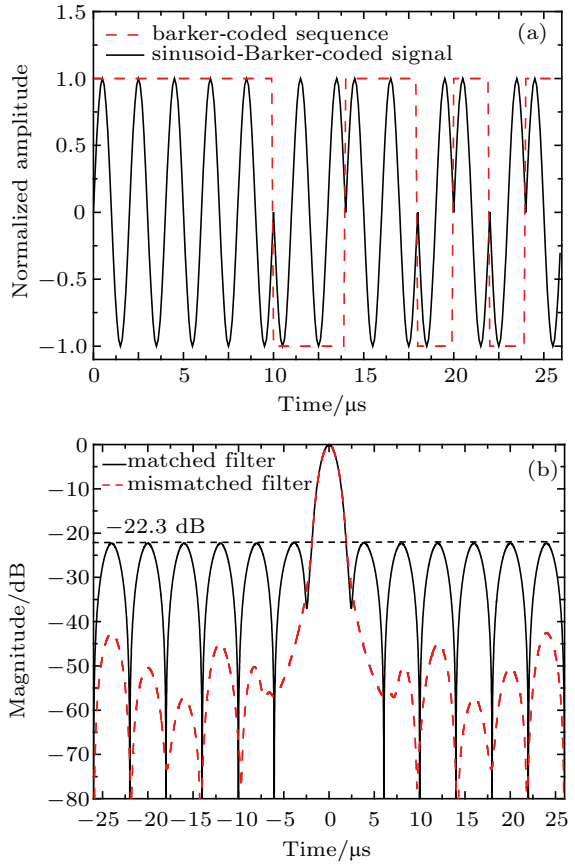


Fig. 2. (color online) (a) Waveforms of the 13-bit Barker-coded sequence and the corresponding sinusoid-Barker coded signal, and (b) output envelopes filtered with the matched and mismatched compression filters.

By taking the inverse Fourier transform of Eq. (8), the time response of the mismatched compression filter can be approximated to

$$h(t) = \sum_{k=-l}^{l} b_l \delta(t - 2T_\mathrm{p}), \tag{9}$$

where l and b_l are the stage number and the coefficient of the filter. By applying the mismatched filter ($l = 8$) to $d(t)$, the envelope of the output plotted in Fig. 2(b) exhibits an obvious side-lobe suppression from -22.3 dB to -42.6 dB. Finally, the MAET signal filtered with the mismatched compression filter can be rewritten as

$$V_\mathrm{d}(t) = \xi' \frac{\partial \sigma(z)}{z \partial z} \otimes R(t) \otimes T(t) \otimes T(-t) \otimes h(t). \tag{10}$$

3. Numerical study

In order to verify the performance of MAET measurement using sinusoid-Barker coded excitation, numerical studies were performed for a four-layered gel model. As illustrated in Fig. 1, the model was immersed in distilled water for acoustic coupling and electrical insulation ($\sigma_\mathrm{w} = 0$ S/m). The density and acoustic speed of water were set to be $\rho = 1000$ kg/m^3 and $c_0 = 1500$ m/s, which were similar to those of the gel phantom. The static magnetic field with the intensity of 0.3 T was assumed to be homogeneous, covering the entire object. A planar piston transducer with a radius of 20 mm and center frequency of 0.5 MHz was placed at $z = 0$. The experimental impulse response of the transducer was measured with a hydrophone, which shows a Gaussian damping packet (short pulse) as illustrated in Fig. 3(a). A cubic gel model with a

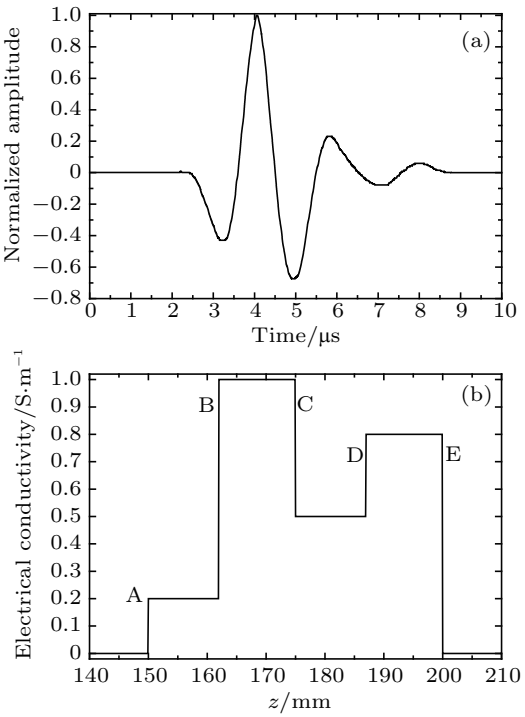


Fig. 3. (color online) (a) Impulse response of the transducer, and (b) conductivity distribution of gel phantom along z direction.

side length of 50 mm positioned at $z = 150$ mm was divided into four layers with a thickness of 1.25 cm and the conductivities of 0.2 S/m, 1 S/m, 0.5 S/m, and 0.8 S/m, respectively, as shown in Fig. 3(b).

With the excitation of a 13-bit sinusoid-Barker coded signal, the MAET signal collected by the electrodes was simulated as plotted in Fig. 4(a). Since the duration of the coded excitation was much longer than the thickness of each layer, long-time wave packets covering the entire signal from 104 μs to 170 μs were generated, which can hardly differentiate the conductivity derivative along the acoustic transmission path at each medium boundary, including the amplitude and polarity. By applying the matched filter to the collected MAET signal, five short wave packets were restored with opposite vibration polarities as plotted in Fig. 4(b), which correspond perfectly to the conductivity interfaces A, B, C, D and E as marked in Fig. 3(b). However, although the packets B, C and E are clear, the packets A and D are not so significant due to the high side-lobe level. Then, the improved mismatched compression filter was used to restore the wave packets with further suppressed side-lobe level and the decoded waveform is shown in Fig. 4(c). Combined with Fig. 3(b), five short packets are clearly shown with the amplitudes and vibration polarities representing the values and directions of conductivity variations along the z direction, which are similar to the collected MAET signal[13] with a single-cycle sinusoidal excitation. Beside the accurate positions and amplitudes as well as the vibration polarities of the corresponding short packets, the SNR is also improved greatly by the low-level of side-lobes, exhibiting the advantages of sinusoid-Barker coded excitation for MAET measurement.

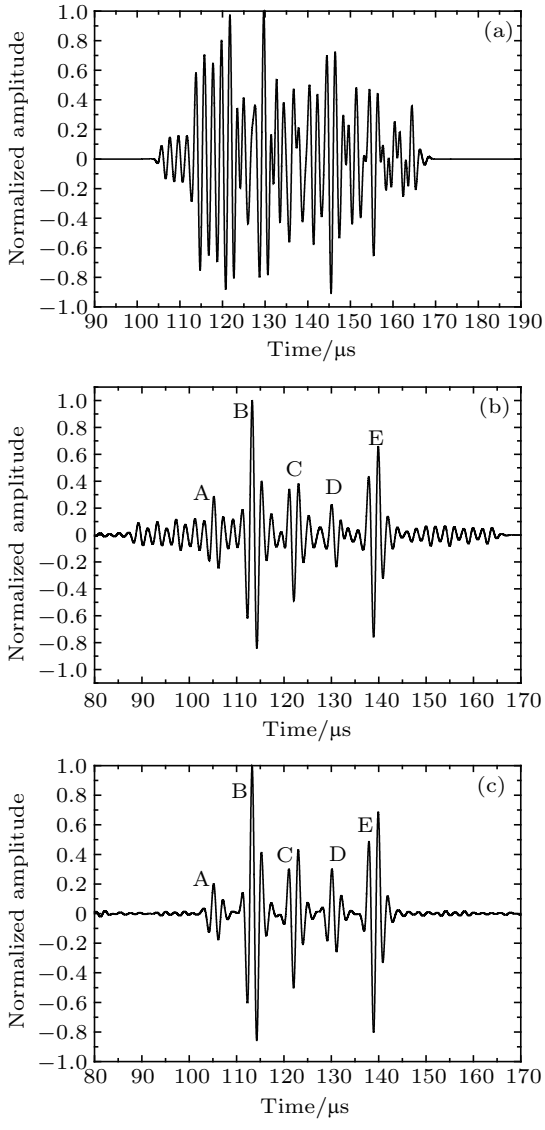


Fig. 4. (a) Simulated waveform of the collected MAET signal with 13-bit sinusoid-Barker coded excitation, and decoded results using (b) matched and (c) mismatched suppression filters.

4. Experiment and results

The sketch map of the experimental MAET measurement system using the 13-bit sinusoid-Barker coded excitation is illustrated in Fig. 5. In distilled water, two silver plate electrodes (50 mm×60 mm) were attached on the front and back sides of a cubic gel phantom. The static magnetic field with an intensity of 0.3 T along the x direction was produced by a pair of permanent magnets (100 mm×100 mm×50 mm) with a distance of 120 mm. A 13-bit Barker code (500 mVpp, PRF 100 Hz, time duration 2 μs) modulated by a single-cycle sinusoidal signal was sent out by a function generator (Agilent 33220A, Agilent Technologies, USA). After being amplified by a power amplifier (53 dB, E&I 2200L, Electronics and Innovation Ltd, USA), the 13-bit sinusoid-Barker coded signal was used to excite the planar piston transducer (radius 20 mm, center frequency 500 kHz). The MAET voltage between the plate electrodes was amplified by a low-noise pre-amplifier (46 dB, NF SA-230F5, 0–10 MHz) and a homemade band-pass filter (46 dB, 370–840 kHz). After 256-time data average, the MAET signal was collected by the digital oscilloscope (Agilent DSO9064A, Agilent Technologies, USA), and saved on the computer for further signal processing.

A three-layered cubic gel phantom with a side length of 50 mm was prepared by sol-gel method in an acrylic mold,[20] and the electrical conductivity of each layer was controlled by adjusting the concentration of NaCl solution, which was measured by the impedance analyzer (Agilent 4294A, Agilent Technologies, USA). In order to analyze the accuracy of MAET measurement, a three-layered gel phantom was prepared layer by layer as shown in Fig. 6. The thickness values of the three layers were set to be 18 mm, 17 mm, and 15 mm with the conductivities of 1 S/m, 0.05 S/m, and 1 S/m, respectively. Because the acoustic characteristics of the gel phantom were similar to biological tissues, the mismatch of acoustic impedance was neglected during acoustic propagation. The transducer and the gel phantom were placed at $z = 0$ and 160 mm, respectively.

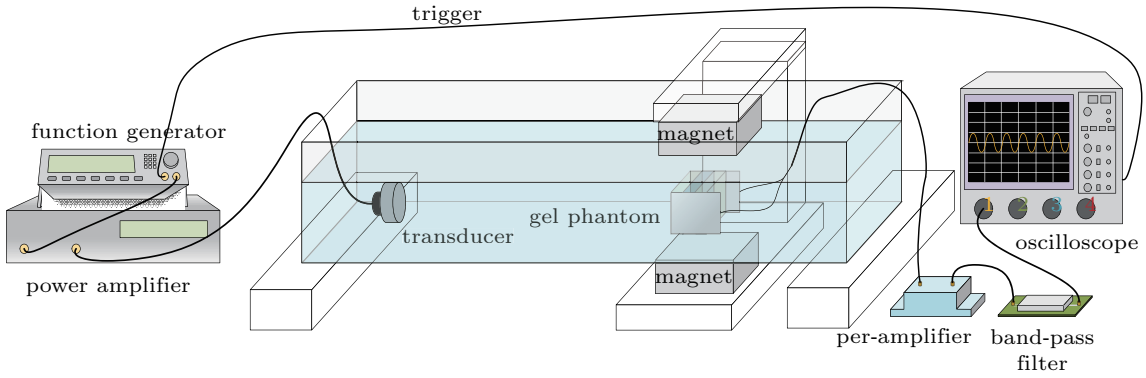


Fig. 5. (color online) Sketch map of the experimental setup of MAET measurement with sinusoid-Barker coded excitation.

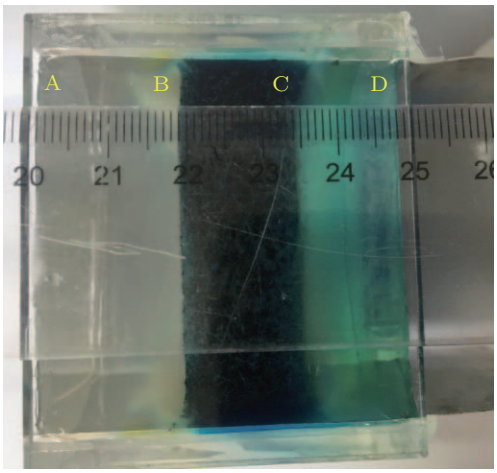


Fig. 6. (color online) Photograph of three-layered gel phantom used in this study.

The collected MAET signal with the 13-bit sinusoid-Barker coded excitation at a peak amplitude of 500 mV is present in Fig. 7(a). Even though several wave packets have different amplitudes and widths, it is not possible to obtain the accurate locations and amplitudes for the boundaries of the layers. By applying the mismatched compression filter, four packets are restored as clearly displayed in Fig. 7(b). The time intervals between the adjacent packets are about 11.7 μs, 11 μs, and 9.8 μs, denoting the thickness values (the value is the time interval multiplied by the acoustic speed) of the three layers in the gel phantom. The vibration polarity of packets A and C is contrary to that of packets B and D, corresponding to the polarity of the corresponding conductivity derivative. Comparing with packet A, the amplitude of packet D decreases for the longer distance attenuation of $\partial\sigma(z)/\partial z$. Due to the decline in the conductivity derivative for the ion motion between the surrounding water and the outer boundaries, the amplitudes of packets A and D are obviously lower than those of the inner packets B and C. In addition, the level of side-lobe is suppressed significantly between the adjacent packets. Also as indicated by the dashed lines in Fig. 7(b), the noise-level of the experimental MAET signal, defined as the amplitude before the first wave packet, is about 4% (−28 dB) relative to the maximum value (normalized 1).

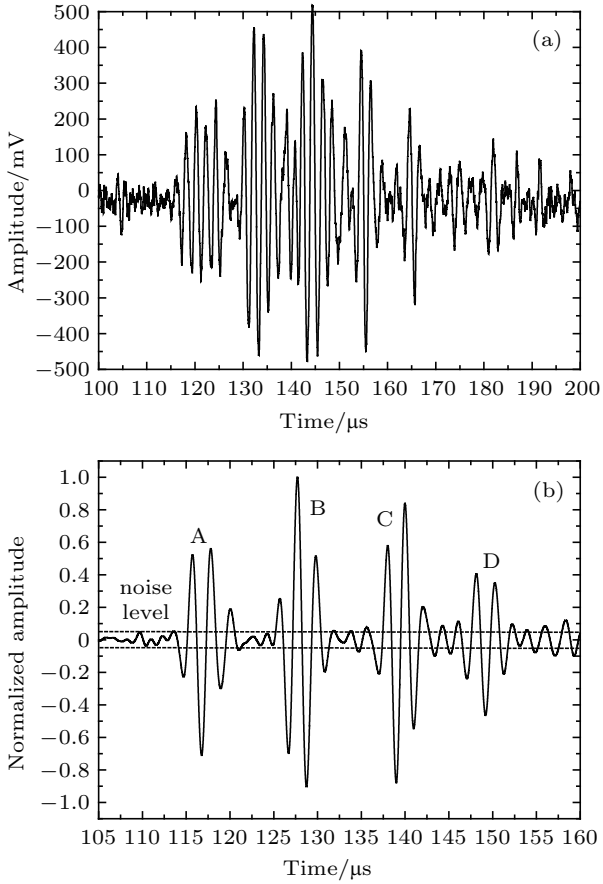


Fig. 7. (a) Waveform of collected MAET signal with 13-bit sinusoid-Barker coded excitation, and (b) normalized result decoded with the mismatched compression filter.

To compare the performance of the collected MAET signal with sinusoid-Barker coded excitation, an experimental measurement using single-cycle sinusoidal excitation was conducted for the same gel phantom The amplitude of the sinusoidal signal was set to be 1 Vpp, which was twice that of the 13-bit sinusoid-Barker coded signal as mentioned above. The waveform collected by the electrodes is plotted in Fig. 8(a) and the normalized result filtered with a digital low-pass filter is also provided in Fig. 8(b) for comparison. Com-

pared with the collected MAET signal with sinusoid-Barker coded excitation as shown in Fig. 7(a), four packets are clearly displayed with the times presenting the positions of the conductivity boundaries of the gel phantom, and the width of each narrower packet is much smaller due to the short-time excitation. Although the transducer is driven with a higher electrical voltage, the peak amplitude (about 300 mV) of the MAET signal is obviously lower than that (about 500 mV) excited with the sinusoid-barker coded signal. After being filtered by the digital low-pass filter, four wave packets are clearly shown in Fig. 8(b), which are similar to those in Fig. 7(b) in terms of the shape and position. However, the noise-level of the restored MAET signal is about 0.1 (−20 dB), which is much higher than the decoded result in Fig. 7(b).

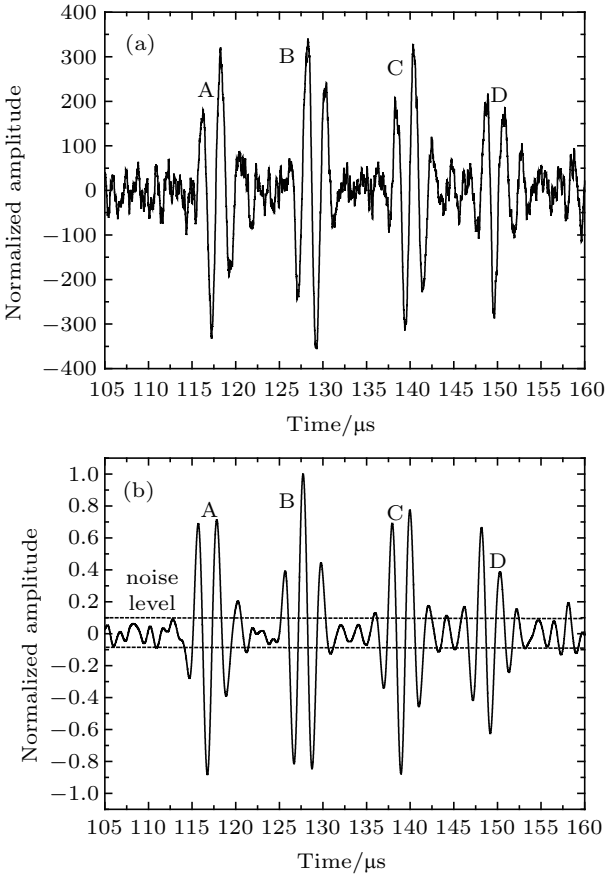


Fig. 8. Experimental waveforms of (a) collected MAET signal with single-cycle sinusoidal excitation and (b) normalized result filtered with a low-pass filter.

5. Discussion

By adjusting the output amplitude of signals, the excitation amplitude dependence of SNR for the collected MAET signals with single-cycle sinusoidal and sinusoid-Barker coded excitations are measured as plotted in Fig. 9. It can be observed that the SNR of the excitations increases accordingly with the increase in the excitation amplitude, while the SNR of the 13-bit sinusoid-Barker coded excitation is about 10 dB higher than that of the single-cycle sinusoidal signal with an identical amplitude. Meanwhile, in order to achieve an MAET signal with an SNR of 20 dB, the amplitudes of 800 and 300 mV for the single-cycle sinusoidal and sinusoid-Barker coded excitations are required. Thus, the improved SNR can be obtained with the excitation of a sinusoid-Barker coded signal at a lower amplitude.

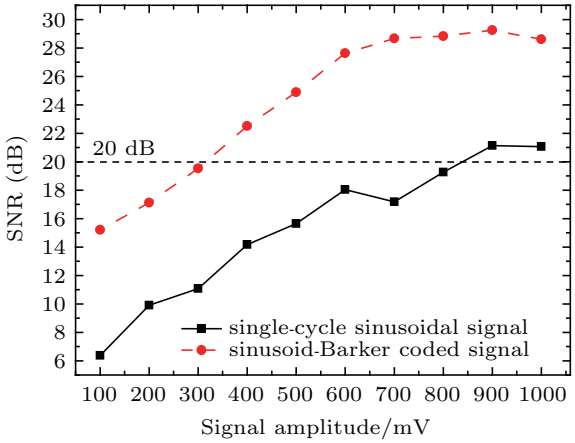


Fig. 9. (color online) Experimental amplitude dependence of SNR for MAET signals with the single-cycle sinusoidal and sinusoid-Barker coded excitations.

Like the other ultrasound imaging methods, the SNR of the MAET signal is dependent on the acoustic energy incident to the medium,[38] and the spatial resolution is determined by the frequency of the sound wave and the radiation pattern of the transducer. With a given pressure amplitude, the energy emission is proportional to the time duration, which is beneficial to enhancing the penetration depth in the safety limit. In this study, the longest 13-bit sinusoid-Barker code excitation is employed to improve the SNR of the MAET signal with a relatively low acoustic pressure, while the spatial resolution of conductivity boundary differentiation can be reduced to a certain extent. The waveform of the simulated ultrasound is the convolution of the driving signal and the impulse response of the transducer with a limited bandwidth, which makes the wave packet wider and reduces the spatial resolution of the experimental system. The modified Weiner filter and Hilbert transformation are employed to reduce the wave packet influence of the impulse response[20] to achieve an improved performance. Although the transducer with a centre frequency of 500 kHz is used in this experiment, the 13-bit sinusoid-Barker code excitation can still be extended to a high-frequency system to improve the spatial resolution. In addition, by combining the linear frequency modulation with the Barker coded sequence, a higher SNR with good spatial resolution is obtained in B-mode sonography,[39] which might be used to improve the performance of MAET measurement for biological tissues in further studies.

6. Conclusions

Based on the principles of MAET and pulse compression technology, theoretical and experimental studies on MAET measurement using sinusoid-Barker coded excitation are conducted for a multi-layered gel phantom. The explicit formula of the MAET signal is derived and simplified for a strong directional transducer, and the corresponding decoded algorithm with side-lobe suppression is also employed to enhance the SNR and spatial resolution. Based on the simulation results of the MAET signal and the decoded waveforms, the performance of wave packet recovery with suppressed side-lobe level is improved by using the mismatched compression filter, which is also demonstrated by the experimental measurements for a three-layered gel phantom. With the sinusoid-Barker coded excitation, the amplitude of the driving signal can be reduced greatly with an SNR improvement of about 10 dB. The value and direction of conductivity variation (conductivity derivative) at tissue boundaries can be achieved by the corresponding amplitude and polarity of the decoded wave packet. The favorable results provide a coded excitation method and a compression algorithm to improve the SNR and spatial resolution for MAET measurement, and suggest the potential applications in biomedical imaging.

References

[1] Peters M J, Stinstra G and Hendriks M 2001 *Electromagnetics* **21** 545
[2] Gielen F L H, Wallinga-de Jonge W and Boon K L 1984 *Med. Biol. Eng. Comput.* **22** 569
[3] Gabriel C, Gabriel S and Corthout E 1996 *Phys. Med. Biol.* **41** 2231
[4] Surowiec A J, Stuchly S S, Barr J R, *et al.* 1988 *IEEE Trans. Biomed. Eng.* **35** 257
[5] Metherall P, Barber D C, Smallwood R H, *et al.* 1996 *Nature* **380** 509
[6] Guo G, Su H, Ding H, *et al.* 2017 *Acta. Phys. Sin.* **66** 164301
[7] Lionheart W R B 2004 *Physiol. Meas.* **25** 125
[8] Wang Q, Wang H, Zhang R, *et al.* 2012 *Rev. Sci. Instrum.* **83** 104707
[9] Li Y, Liu G, Xia H, *et al.* 2018 *IEEE Trans. Magn.* **54** 5100704
[10] Zengin R and Gencer N G 2016 *Phys. Med. Biol.* **61** 5887
[11] Roth B J and Schalte K 2009 *Med. Biol. Eng. Comput.* **47** 573
[12] Kunyansky L, Ingram C P and Witte R S 2017 *Phys. Med. Biol.* **62** 3025
[13] Han W, Shah J and Balaban R S 1998 *IEEE Trans. Biomed. Eng.* **45** 119
[14] Han W 1999 *Ultras. Imaging.* **21** 186
[15] Xu Y and He B 2005 *Phys. Med. Biol.* **50** 5175
[16] Li Y, Liu Z, Ma Q, *et al.* 2010 *Chin. Phys. Lett.* **27** 084302
[17] Guo G, Ding H, Dai S, *et al.* 2017 *Chin. Phys. B* **26** 084301
[18] Ammari H, Qiu L, Santosa F, *et al.* 2017 *Inverse Problems* **33** 125006
[19] Haider S, Hrbek A and Xu Y 2008 *Physiol. Meas.* **29** S41
[20] Zhou Y, Ma Q, Guo G, *et al.* 2018 *IEEE Trans. Biomed. Eng.* **65** 1086
[21] Kunyansky L 2012 *Inverse Problems* **28** 035002
[22] Ammari H, Grasland-Mongrain P, Millen P, *et al.* 2015 *J. Math. Pures App.* **103** 1390
[23] Polydorides N 2018 *Physiol. Meas.* **39** 044003
[24] Grasland-Mongrain P, Mari J M, Chapelon J Y, *et al.* 2013 *IRBM* **34** 357
[25] Renzhiglova E, Ivantsiv V and Xu, Y 2010 *IEEE Trans. Ultrason., Ferroelectr., Freq. Control.* **57** 2391
[26] Pedersen M H, Misaridis T X and Jensen J A 2003 *Ultrasound Med. Biol.* **29** 895
[27] Dantas T M, Costa-Felix R P B and Machado J C 2018 *Appl. Acoust.* **130** 238
[28] Sun Z, Liu G, Xia H, *et al.* 2018 *IEEE Trans. Ultrason., Ferroelectr. Freq. Control.* **65** 168
[29] Sun Z, Liu G and Xia H 2017 *Chin. Phys. B* **26** 124302
[30] Sun Z, Liu G and Xia H 2018 *Chin. Phys. Lett.* **35** 014301
[31] Nowicki A, Klimonda Z, Lewandowski M, *et al.* 2006 *Ultrasonics* **44** 121
[32] Hansen K L, Udesen J, Gran F, *et al.* 2009 *Ultraschall. Der. Med.* **30** 471
[33] Nowicki A, Trots I, Lewin P A, *et al.* 2007 *Ultrasonics* **47** 64
[34] Xiang L, Zhao H and Gao S 2009 *Ultrasound. Med. Biol.* **35** 94
[35] Sun X, Wang X, Zhou Y, *et al.* 2015 *Chin. Phys. B* **24** 014302
[36] Grasland-Mongrain P, Destrempes F, Mari J M, *et al.* 2015 *Phys. Med. Biol.* **60** 3747
[37] Rihaczek A W and Golden R M 1971 *IEEE Trans. Aero. Elec. Sys.* **AES-7** 1087
[38] O'Donnell M 1992 *IEEE Trans. Ultrason., Ferroelectr. Freq. Control.* **39** 341
[39] Fu J, Wei G, Huang Q, *et al.* 2014 *Biomed. Signal. Proces.* **13** 306